Enhancing Skin Cancer Detection Through an AI-Powered Framework by Integrating African Vulture Optimization with GAN-based Bi-LSTM Architecture

N.V. Rajasekhar Reddy[1], Dr Araddhana Arvind Deshmukh[2], Dr. Vuda Sreenivasa Rao[3], Dr Sanjiv Rao Godla[4], Prof. Ts. Dr. Yousef A.Baker El-Ebiary[5], Liz Maribel Robladillo Bravo[6], R. Manikandan[7]

Professor, Department of Information Technology, MLR Institute of Technology, Hyderabad[1]

Head and Associate Professor, Department of Artificial Intelligence and Data Science, Marathwada Mitra Mandal College of Engineering-Affiliated to Savitribai Phule Pune University[2]

Associate professor, Department of Computer Science and Engineering, Koneru Lakshmaiah Education Foundation, Vaddeswaram, AP, India[3]

Professor, Department of CSE (Artificial Intelligence & Machine Learning), Aditya College of Engineering and Technology-Suraplem, Andhra Pradesh, India[4]

Faculty of Informatics and Computing, UniSZA University, Malaysia[5]

Universidad César Vallejo, Peru[6]

Research Scholar, Vel Tech Rangarajan Dr. Sagunthala R&D Institute of Science and Technology, Avadi, Chennai-600062, Tamil Nadu, India[7]

***Abstract*—One of the more prevalent and severe cancer kinds is thought to be skin cancer. The main objective is to detect the melanoma in initial stage and save millions of lives. One of the most difficult aspects of developing an effective automatic classification system is due to lack of large datasets. The data imbalance and overfitting problem degrades the accuracy. In this proposed work, this problem can be solved using a Generative Adversarial Network (GAN) by generating more training images. Traditional RNNs are concerned with overcoming memory constraints. By using a cyclic link on the hidden layer, these models attain Long short-term memory. However, RNNs suffer from the issue of the gradient disappearing, which affects learning performance. To overcome these challenges this work proposes Bidirectional Long Short-Term Memory (Bi-LSTM) deep learning framework for skin cancer detection. The dataset which is collected from the International Skin Imaging Collaboration were used in image processing. A novel metaheuristic enthused by the routine of African vultures is proposed in this proposed work. The African Vulture Optimisation Algorithm (AVOA) algorithm is designed to select optimum feature of skin image. The accuracy of the proposed method obtains 98.5%. This comprehensive framework, encompassing GAN-generated data, Bi-LSTM architecture, and AVOA-based feature optimization, contributes significantly to enhancing early melanoma detection.**

***Keywords*—Skin cancer; generative adversarial network; Bi-LSTM; African Vulture Optimisation (AVO); deep learning (DL)**

I. INTRODUCTION

Skin cancer has become difficult to diagnose because of apparent similarities. Melanoma is the well-known type of skin cancer, have been caused for a significant number of deaths in recent years. Recent surveys show that in contrast with various cancer types, the number of skin cancer patients is growing annually. Melanocytes, the skin external cells, are affected by it. It has several cell types that result in the skin becoming darker. It irregularly comes in a variety of dark tones. It can also be noticed on the skin in colorless or in shades of rosy pink in color, royal purple, azure, and more. It is more deadly and hazardous because it spreads quickly. Melanoma can be discovered everywhere on the human body, despite the fact that it typically develops on the lower limb's backside [1]. According to data from the World Health Organization (WHO), there are several thousand cases worldwide with a high risk of death by the year 2020. According to that, 324,635 new cases have been reported globally, of which 57,043 have resulted in death. The researcher also demonstrate that, of every 100 persons with melanoma, 18 will not survive [2].Melanocytes in the epidermal layer have the potential to produce excessive amounts of melanin at a high rate in several circumstances. For instance, melanin is produced when strong UV radiation from sunlight is exposed for an extended period of time. Melanoma, a deadly kind of skin cancer, is the outcome of melanocytes' unusual growth. For successful treatment of melanoma, an early diagnosis is crucial. The survival percentage for 5 years is approximately 92% if the skin cancer is sensed at an earlier phase [3]. Accurate and timely diagnosis of melanoma, a deadly form of skin cancer, remains a pressing challenge in the field of dermatology and healthcare. Despite advancements in medical technology, the current diagnostic methods are often subjective and error-prone, leading to delayed diagnoses and poorer patient outcomes. The need for a more reliable and efficient approach to melanoma detection is evident, especially considering the increasing incidence of skin cancer worldwide. This research endeavors to address

these critical issues by developing an automated melanoma detection system that leverages the power of deep learning and convolutional neural networks.

Historically, skin cancer diseases have been diagnosed and detected by manual examination and inspection by sight. These methods for skin doctor to visually assess and screen lesion photographs are time-consuming, difficult, and error-prone [4]. Use of the ABCDE rule, which stands for asymmetry, boundaries, color, diameter, and evolving, is a typical way for spotting melanomas [5]. To diagnose melanoma, these warning indicators are monitored. The first warning indicator is a mole that is very asymmetrical or has uneven border patterns, as well as one that is larger than 6 mm in diameter and has an odd color. All of these indicators are tracked in order to study how researcher changes over time which determines the presence of melanoma. This methodology could be inaccurate and prone to measurement mistakes [6]. Effective feature extraction, classifiers, and color capture are required for the detection of skin lesion images. Recent developments have made it possible to diagnose melanoma accurately by molecular dermatopathology, which necessitates a discussion between a pathologist and a dermatologist. Even though the majority of dermatopathologists can determine the histological evaluation of melanocytic lesions by performing a traditional microscopic examination, some melanocytic neoplasms known as typical melanocytic proliferations require expert opinion before categorized as benign or malignant. The investigation of the histopathological features in relation to the clinical and microscopy data is also required because of this. If molecular diagnostics is used incorrectly to decide whether a condition is benign or malignant, it may also be deceptive and lose some of its greatest value [7]. However, this method can only be executed effectively by skilled medical specialists. These complications boost the scientific people to generate innovative systems for melanoma visualization and diagnosis. Melanoma cancer is diagnosed with the use of a computer-aided diagnosis (CAD) system. CAD diagnostic tool evidence can be utilized as a backup diagnosis for melanoma malignancy [8]. The expanding use of machine learning and AI in the disciplines of medical and health care has attracted a lot of study attention in recent years [9]. Clinical image of skin lesions with the existence of artefacts such as hair, veins, and texture and other issues might be challenging to identify melanoma lesions away from non-melanoma lesions. Consequently, the need for imagery preparation is crucial [10]. Early detection has been proven to significantly improve patient survival rates, with a five-year survival rate of approximately 92% when melanoma is detected at an earlier stage. By addressing the shortcomings of current diagnostic methods, this research aims to contribute to saving lives and reducing the burden of melanoma on individuals and healthcare systems.

Convolutional neural networks with deep learning recently entered the field of image-based skin cancer diagnosis and demonstrated diagnostic performance comparable to that of dermatologists. It would be ideal if doctors had assistance in the diagnosis of difficult-to-diagnose melanomas with unique localizations and uncommon subtypes [11]. The segmentation is a vital step in creating an automated melanoma detection system. However, when there is no variation in image contrast or when there are just slight variations in illumination in the image content, the region of interest or thresholding-based algorithms perform well [12]. ResNet-50 Convolutional Neural Network (CNN) architecture was designed. CNN model employed a varied learning rate for each CNN layer. To slow down learning rates, novel techniques based on the cosines function is applied. The success percentage for the categorization had a sensitivity rate of 82.3% [13]. In deep CNN SoftMax classifier were used. This approach worked effectively for lesion images that were blurry and had many sizes. This method was calculated using skin lesion samples from PH2 and ISIC 2018 and yielded respectable accuracy and dice coefficients of 95% and 93%, for each [14].

The existing diagnostic methods for melanoma are beset by several limitations that hinder their effectiveness. Manual examination, reliant on visual inspection, is not only time-consuming but also susceptible to human subjectivity. The widely-used ABCDE rule, which assesses asymmetry, boundaries, color, diameter, and evolution, can introduce errors due to its reliance on qualitative observations. The presence of noisy images with artifacts like hair, veins, and variations in color makes accurate diagnosis even more challenging. These limitations underscore the need for a more objective, automated, and robust approach to melanoma detection. And also often struggle to accurately detect and segment melanoma lesions due to factors such as inadequate image segmentation, vanishing/exploding gradients in deep learning architectures, and difficulty in handling noisy images with variations like hairs or color changes. The current landscape of melanoma diagnosis is characterized by a conspicuous gap between the pressing need for accurate and timely detection and the limitations of existing methods. While deep learning and CNNs have shown immense potential in image-based tasks, their application to dermatology, especially for melanoma detection, remains a relatively unexplored territory. This research aims to bridge this gap by introducing an innovative approach that combines advanced technology with the critical domain of skin cancer diagnosis. Moreover, certain techniques suffer from computational intensity during feature extraction, leading to time-consuming analyses. In this work AI driven African Vulture optimization with GAN based Bi-LSTM deep framework for melanoma detection is projected. The primary contributions of the suggested work include:

- Data Collection and GAN Augmentation: The utilization of skin cancer images from the International Skin Imaging Collaboration (ISIC 2018) addresses the challenge of limited data availability. The integration of Generative Adversarial Networks (GANs) to generate additional synthetic images serves as a solution for data imbalance, enhancing the diversity and size of the dataset.
- Advanced Preprocessing Techniques: The implementation of Contrast Limited Adaptive Histogram Equalization (CLAHE) and Weiner filtering on input images aids in enhancing image quality and reducing unwanted artifacts such as hair, veins, and

noise. This preprocessing pipeline ensures that the subsequent analysis is based on clean and standardized data.

- Precise Skin Contour Segmentation: The application of Kapur thresholding for skin contour segmentation generates binary images that precisely isolate the skin lesions from the background. This step is pivotal in isolating the region of interest and improving subsequent feature extraction.
- Optimal Feature Selection: The introduction of African Vulture Optimization (AVO) algorithm for selecting optimal features from skin images adds a novel contribution. This technique helps to streamline and enhance the feature extraction process, potentially leading to more effective and efficient classification.
- Hybrid CNN-Bi-LSTM Architecture: The design of a Convolutional Neural Network (CNN) with Bidirectional Long Short-Term Memory (Bi-LSTM) layers offers a robust architecture for detecting melanoma. This combination enables the model to capture both spatial features from images and sequential patterns, potentially improving accuracy and diagnostic capabilities.

Overall, the key contributions encompass data augmentation, advanced preprocessing, precise segmentation, innovative feature selection, and a sophisticated deep learning architecture, collectively aiming to boost the accuracy and effectiveness of early melanoma detection and diagnosis. The leftover portion of this work is organised as follows: Section II contains comparable work as well as a thorough examination of them. Section III contains information about the problem statement. The proposed AVO-CNN architectures are discussed in detail in Section IV. In Section V, the outcomes of the experiments are presented and examined, and a full comparison of the suggested strategy to current best practises is given. Section VI, is the final section, where the paper is concluded.

II. Related Works

Albert [15] proposed the combination of Predict-Evaluate-Correct K-fold (PECK) algorithms and Synthesis and Convergence of Intermediate Decaying Omnigradients (SCIDOG) . MED-NODE data set were used to diagnose melanomas via digital image analysis. In the PECK algorithm 153 non-dermoscopic images of lesion were deep ensembled. On that data the state-of-the-art methods were educated and estimated. Considerable improvement in diagnostic performance over the most effective earlier approaches was achieved through introspective learning of the PECK ensemble to increase precision from sparse but high-dimensional training data.

Jiang, Li, and Jin [16] introduced a light-weight based deep learning outline called DRANet to distinguish between 11 dissimilar categories of skin diseases using a factual histopathology data set amassed over the past ten years. DRANet outperforms baseline models (such InceptionV3, ResNet50, VGG16, and VGG19) by a significant margin with identical parameter sizes and comparative accuracy with fewer parameters. Vanishing/exploding gradients are a concern, and several stacked layers can occasionally have substantial training error. Shorfuzzaman [17] suggested a comprehensible ensemble stacked structure with CNN for early malignance skin tumor detection. Multiple sub-models of CNN which performs the similar classification are collected in the loading ensemble outline, which employs the transfer learning idea. All of the predictions from the sub-models are combined into a novel model termed a meta-learner, which produces the final prediction outcomes. Stacking ensemble model was trained and validated using skin lesions Kaggle dataset obtained over the International Skin Image Collection. The dataset includes 1497 and 1800 pictures of benign and cancerous moles, respectively. According to evaluation results, the ensemble model has better accuracy of 95.76%, sensitivity of 96.67%, and AUC of 0.957. Low-quality prediction results from inadequate image segmentation.

Wei, Ding, and Hu [18] suggested a simple model for detecting skin cancer that uses feature discrimination and the fine-grained classification principle. Two sets of training samples of the recognition model are first introduced in Lightweight CNN. This technique can extract additional discriminatory lesion characteristics and progress the performance in a bit of time. Next, two sets of output from CNN unit are used for training of two-feature group and differential networks simultaneously. Accuracy of 96.2% achieved by fusion performance can be improved by efficient discrimination network. Wang et al. [19] proposed an information that alert deep framework that imposes several clinical knowledge to feature segmentation and melanoma recognition unit. Lesion-based pooling and shape extraction (LPSE) structure is developed to move the data gained from image partition to detection unit. Also transmit data from recognition to segmentation units simultaneously. An efficient diagnosis guided feature fusion (DGFF) approach and recursive learning, is proposed which iteratively enhances the learning capability and boosts the performance It is more time consuming and labor intensive.

A lot of computer-aided diagnosis mechanisms have been created in the earlier. Due to the skin lesion images complicated visual qualities, which include irregularly shaped features and fuzzy edges, had trouble performing. Adegun and Viriri [20] suggested a deep learning technique to automate melanoma lesion detection and segmentation that gets over these restrictions. For efficient learning and feature extraction, an enhanced encoder-decoder structure with independent networks coupled through a number of skip pathways is proposed. This network increases the level of semantics of the feature encoder maps closest to decoder. In addition, SoftMax and Lesion-classifier were used. On International Skin on Biomedical Imaging (ISBI) 2017 dataset, proposed approach was accurate, with 95% and 92% dice coefficients. While on Pedro Hispano (PH2) dataset, it had an accuracy of 95%, dice coefficient of 93%. Some current state-of-the-arts are outperformed by this approach. This method needs better accuracy.

Manzo and Pellino [21] implemented deep CNN structures using prior training for visual representation with the aim of

predicting melanoma in skin lesions. To extract image features using a transfer learning strategy. The transfer learning features were then used in a grouping of classifications framework. The model precisely learns different classifiers then uses statistical techniques to grouping the supplied predictions. The primary weakness is the computing difficulty associated with the features extraction step, which is known to be time-consuming, especially as the amount of data to be analyzed increases. A hybrid classification method was created by İlkin et al. [22] combining a heuristic optimization technique and the SVM algorithm. It has certain advantages, but it also has some big disadvantages. Images with noise, such as hairs or colour changes, degrade performance. When a wounded area extends beyond the image's boundaries, the classifier's effectiveness in capturing the model's acquired characteristics diminishes.

III. PROBLEM STATEMENT

When applying classification methods on Melanoma images, data imbalance was challenging. Data imbalance causes overfitting problem [16], poor accuracy [20] and training error. Overfitting problem can be solved by increasing the size of dataset which accomplished through GAN (Generative Adversarial Network). CLAHE and Weiner filter which potentially remove noises and artifacts interfering with the classification. The existing work suffers from the issue of the gradient disappearing, which affects learning performance. To overcome these challenges this work proposes Bi-LSTM Deep Learning framework for skin cancer detection. The time consumption could be reduced by implementing African Vulture Optimization (AVO).

IV. PROPOSED GAN BASED BI-LSTM WITH AVO

Research must automatically discover class-preserving changes to generate valid and representative samples in order to combat the imbalanced class problem and further improve classification accuracy. However, the samples of skin lesion should have high resolution for classification to detect the presence of malignant in skin lesion. Fig. 1 illustrates the proposed GAN-Bi-LSTM with AVO.

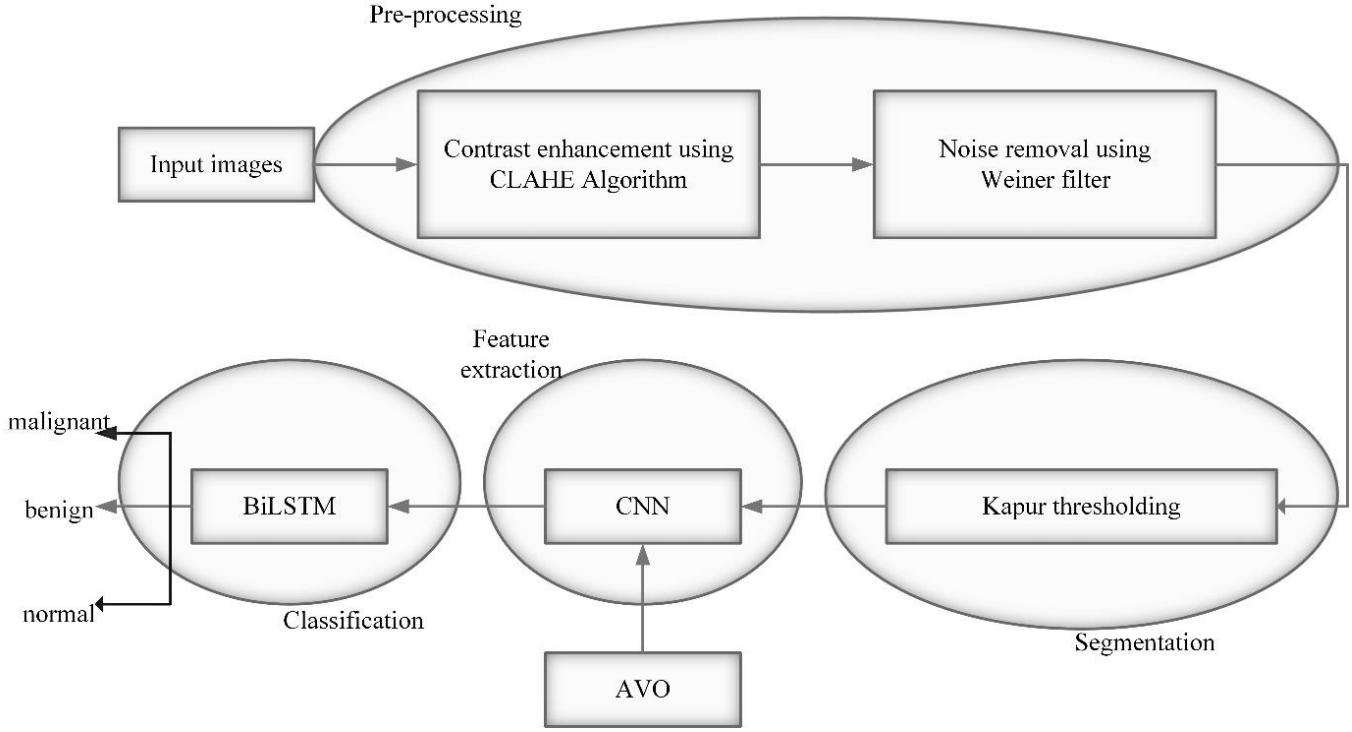

Fig. 1. Proposed AVO with GAN based Bi-LSTM.

The skin cancer images are grouped from ISIC 2018 and the fake images were generated using GAN to overpower the problem of data imbalance. The input images were preprocessed with CLAHE algorithm then filtered by Weiner filter to eliminate unwanted artifacts such as hair, veins and other noise factors. Then the skin contour is segmented by kapur threshold as binary images. The special features of skin images were extracted and optimum feature is selected in African Vulture Optimization (AVO). CNN with Bi-LSTM were designed to detect the melanoma from the skin lesion.

A. Data Collection

The International Skin Imaging Collaboration (ISIC 2018) provided the dataset for research which has challenges [23]. The objective is to automatically detect melanoma using dermoscopic pictures. There are three components to the challenge: Segmentation of Lesion, Visual Dermoscopic Features/Patterns Detection & Localization, and melanoma Classification. The proposed concentrate on the third job, which requires you to categorize lesion images into three different groups: melanoma, benign and normal. The dataset contains of images with multiple resolution. Although researcher chooses the test images at random, make sure that the class distribution is maintained and that the proportion of images from each class is comparable in the train and test sets.

B. GAN-based Data Augmentation

GAN is one of the generative techniques in deep learning. GAN framework consists of two neural networks. They are simultaneously guided discriminator and generator. A generator network G produces images from noise n and given to discriminator network D which identify the difference between real image y and synthetic images generated by generator G. The images with better resolution are ready for further process. If the image produced by generator is not identical to the real image again it is given to discriminator and generator network. The construction of GAN is depicted in Fig. 2.

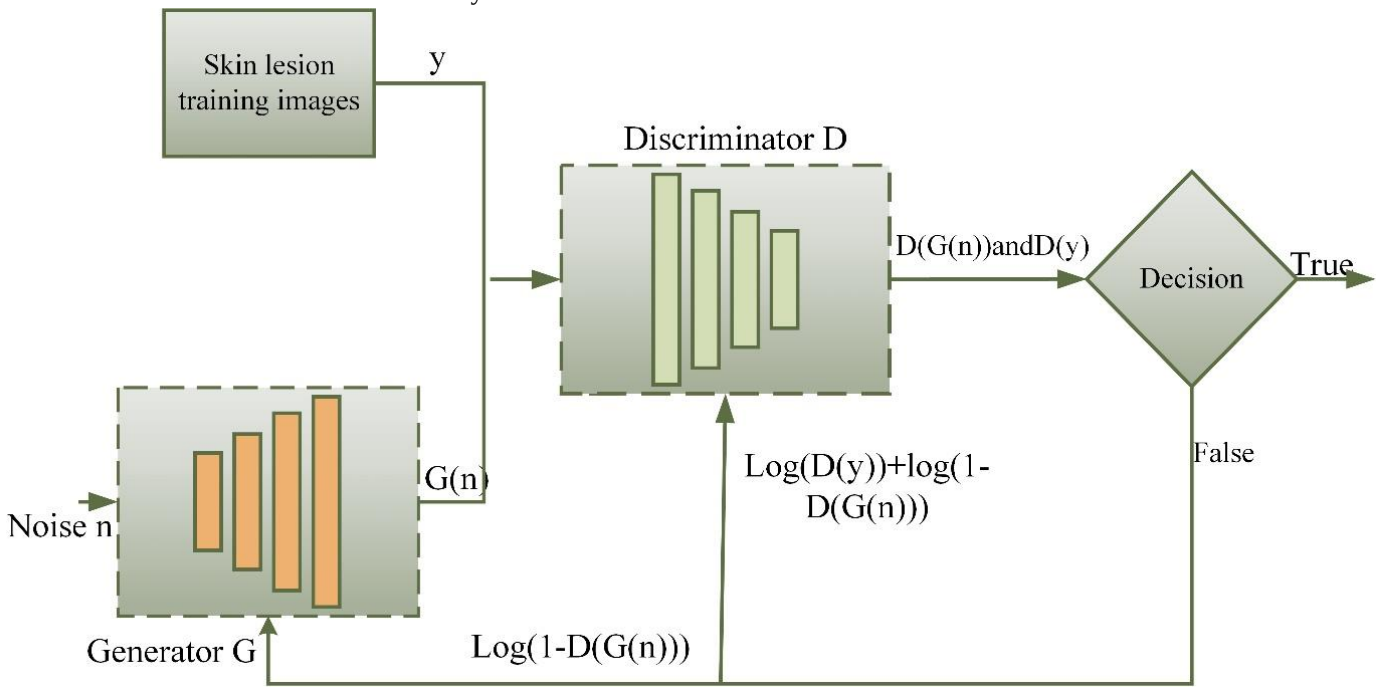

Fig. 2. Construction of GAN.

1) Generator: A convolution neural network serves as the generator based on unsupervised learning. The generative model that creates images that is comparable to the training images. In order to produce samples with a distribution that is similar to that of real samples, this artificial neural network assesses the probable distribution of the raw data and updates its parameters. The generator gets noise that is random and provides outputs information. There is some noise in the distribution as well. Now, the distribution of noise can be normal, uniform, or any other type. The generator feeds the discriminator network with its fake image output, and the discriminator performs its training and determines whether the input is real or fake.

2) Discriminator: A convolution neural network is a discriminator with supervised learning. It works as binary classifier that is learned on training images and forecasts whether the test image is a genuine or one that has been manufactured. Real images from the original training samples as well as generated image produced by the generator are included in the discriminator's training samples. During the training process, these fake images are utilised as negative examples. The generator works effectively creating genuine images. Only the discriminator can fail to discriminate among the first and generated samples.

3) Loss function: The loss function is found to evaluate error then it restores variations. It is specified for the generator as well as the discriminator. The difference among the delivery of data generated by the generator and the delivery of the real images is calculated using the GAN loss function [24]. The discriminator tries to lower the negative log-likelihood. However, the generator just maximises negative log-likelihood since it wants to trick the discriminator. Since it can use the discriminator's cost function, the discriminator loss function is given in Eq. (1) as:

$$\max_D V(G,D) = E_{y\sim P_{data}(y)}[\log D(y)] + E_{y\sim P_n(n)}[\log(1 - D(G(n)))] \quad (1)$$

To minimize log (1- Des (Gen (z))), the Generator is trained. It produces images as similar to the real training images as possible. The generator loss function is expressed in Eq. (2) as,

$$\min_G V(G,D) = E_{y\sim P_n(n)}[\log(1 - D(G(n)))] \quad (2)$$

The generator and discriminator are optimized by the following Eq. (3),

$$\min_G \max_D V(D,G) = E_{y\sim P_{data}(y)}[\log D(y)] + E_{n\sim P_n(n)}\left[\log\left(D(G(n))\right)\right] \quad (3)$$

C. Image Preprocessing

Progressed images with interrelated masks for rotation, resizing, reflection and brightness were designed for each image. The less quality of the input lesion images delivered by electronic detectors restricts detection and evaluation. Up

sampling was used on the lesion images to solve the imbalanced class distribution. The ISIC2018 dataset was partitioned into three distinct groups for training, testing, and analysis to deal with the overfitting problem carried on by the smaller quantity of used training images.

1) Image enhancement using contrast-limited adaptive histogram equalization (CLAHE): The pixel spreading can be realised in the image histogram. The contrast of image can be improved by rearranging the pixel distribution. Histogram equalisation, which can improve the variety of every pixel grey amount, is a mapping transformation of the original image 's grey level. So that image contrast is enlarged. An adaptive histogram equalisation (AHE) technique has a tendency to overamplify noise in the areas of the image that are reasonably uniform. The CLAHE approach was suggested as a solution to this issue. Divide the image into parts that are non-overlap. Typically, the area dimension is established to 8 by 8. Obtain the histogram for each region, then trim the histogram using the threshold. By clipping of histogram with a predetermined threshold prior to calculating the Cumulative Distribution Function (CDF), the CLAHE algorithm attains the purpose of restricting the amplification [25]. This restricts the transformation function's slope as well. Redistribute pixels, then uniformly Spread the values of the clipped pixels under the histogram. local histogram equalisation is carried out on each region is shown in Fig. 3.

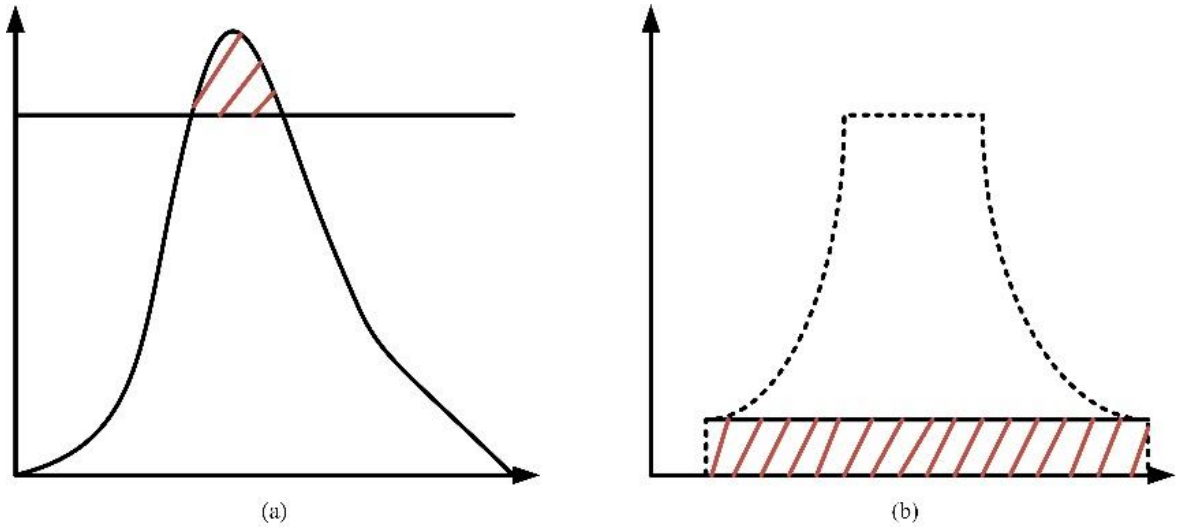

Fig. 3. Histogram equalization (a) before cutting (b) after cutting.

The linear interpolation is used to reconstruct the pixel value. Consider v as a grey value of image's sample point R and v' is the new grey value of that by performing linear interpolation. Let the sample points for surrounding regions are R1, R2, R3 and R4.gr(v)is grey-level mapping for v.

The new grey value for pixels in the corners corresponds to the grey-level mapping for v. The new grey

value is expressed in Eq. (4),

$$v' = gr_1(v) \tag{4}$$

New grey value of pixels in edges is the mapping of grey level for v of two samples is expressed in Eq. (5),

$$v' = (1-\alpha)gr_1(v) + \alpha gr_2(v) \tag{5}$$

New grey value of pixels in centre is the mapping of grey level for v of four samples is given in Eq. (6),

$$v' = (1-\beta)\big((1-\alpha)gr_1(v) + \alpha gr_2(v)\big) + \beta((1-\alpha)gr_3(v) + \alpha gr_4(v)) \tag{6}$$

where, the normalized distances are α and β with regards to the point R1.

Due to the reason that a few of the images have tiny pixel counts and which need to be resized. This leads to considerable changes in the image's luminance and size. There are many sets of parameters for various acquisition instruments. All pixel density was normalized within the range [-1, 1] to ensure that the data were reliable and noise-free. Eq. (7)'s normalization computation made the model less sensitive to minute weight changes. Normalization of image I_{Norm} is given in Eq. (7) as,

$$I_{Norm} = (I - min_i)\left(\frac{2}{max_i - min_i}\right) - 1 \tag{7}$$

Where, min_i and max_i are minimum image and maximum image.

2) Noise removal by wiener filters: The method used to remove unwanted data from the image is statistical. It achieves ideal trading among noise flattening and reverse filtering which filter the blurring and noise existing in the image [26].

Filter function is given in Eq. (8) as,

$$f(y,z) = \left[\frac{H(y,z)^*}{H(y,z)^2 + \left[\frac{S_n(y,z)}{S_i(y,z)}\right]}\right] G(y,z \tag{8}$$

Where G(y,z) represents degraded image, H(y,z) is degradation function, $S_n(y,z)$ is a power spectra of noise and $S_i(y,z)$ shows the original image's power spectrum.

D. Image Segmentation by Kapur Thresholding Technique

When taking a picture in many medical circumstances, negative impacts imposed to the skin image, causing image examination challenging for the computational approaches. In the case of input, portion of the skin image is essential and the rest of the image is not significant. To eliminate these negative consequences, kapur thresholding was applied. The image thresholding is used to keep the essential parts and eliminate the unwanted. Image thresholding is an image separation method that converts an image's pixel values to zero and one. In general, a threshold level value for the picture pixel points which overall value as threshold for all or each pixel may have different threshold value. The image's pixels are then compared to that level, and if the pixel intensity is more than the threshold, it is turned white; otherwise, it is turned black. As an outcome, a grayscale image is transformed into an image that is binary (black and white). Typically apply thresholding to choose portions of an image and eliminate those that aren't significant to us. Consider an image with L levels and N pixels ranging between 0 and L-1, If g(j) indicates the gray-level number and j describes image existences then median value of image is given in Eq. (9).

$$Mean = g(j)/N \tag{9}$$

The dermoscopy pictures were threshold using the Kapur technique. This procedure determines the limit using entropy T(u) boosting and histogram data, which can be computed using Eq. (10) to (14):

$$Max\ T(u) = A(0,u) + A(u,L) \tag{10}$$

$$\text{Where} \quad A(0,u) = -\sum_{j=0}^{u-1} \frac{P_j}{W_0} \ln \frac{P_j}{W_0} \tag{11}$$

$$W_0 = \sum_{j=0}^{u-1} P_j \tag{12}$$

$$A(u,L) = -\sum_{j=u}^{L-1} \frac{P_j}{W_1} \ln \frac{P_j}{W_1} \tag{13}$$

$$W_1 = \sum_{j=u}^{L-1} P_j \tag{14}$$

The ideal threshold value is calculated by maximizing the function $T(u)$ and u number of grey levels was considered.

E. Extraction and Classification using AVO based CNN -Bi-LSTM

1) Feature extraction using CNN: Convolution, fully connected (FC) and pooling layers are stacked to form a CNN architecture. Each convolution layer has a set of filters that are learnable which is to acquire local features from the image being processed using the knowledgeable filters. It is probable to reduce computing complication while improving performance by constructing filters that conduct convolution actions based on two important ideas, namely weight division and local linking. The pooling layer is in charge of the down sampling process. One of the pooling layer's distinguishing characteristics is that it reduces the overall dimension of the image and avoids overfitting. Typically, FC layers are employed in the final CNN layer design to learn features returned by the layer of convolution; it is then utilised to construct the output.

2) Feature selection using African vulture optimization (AVO): The latest metaheuristic technique developed through vulture tracking is called AVO. Vultures are a type of bird that may be found all over the world. Vultures are typically carnivorous; nevertheless, these birds are unable to divide the flesh and must rely on a different meat-eating to do it. African vultures may reach altitudes that exceed 11000 meters, and they travel great distances and rotate to locate food. They usually have difficulties after discovering a food source. The weaker vultures encircle the healthier vultures, delaying their activity; as that vulture fatigue, they begin to seek food. This way of living motivates to create a novel metaheuristic approach for tackling an optimization issue [27].

Stage 1: Increasing the size of the population, achieving similar values for each vulture, identifying the greatest vulture in each group, and selecting the best result for each group. This is explained in Eq. (15).

$$S(k) = \begin{cases} Best\ vulture_1, if\ Z_k = f_1 \\ Best\ vulture_2, if\ Z_k = f_2 \end{cases} \tag{15}$$

f1 and f2 specify the parameters that are examined before to optimization, which must be between 0 and 1, where f1+f2=1.

Stage 2: Calculating the vulture famine rate. Vultures soar over the sky in quest of food. When there is insufficient energy, the vulture approaches stronger to grab a free meal. This is mathematically modelled in Eq. (16) and (17) as,

$$V = (2 \times \delta + 1) \times N \times \left(1 - \frac{iter_k}{max_{iter}}\right) + l \tag{16}$$

Where,

$$l = d \times \left(\sin\left(\frac{\pi}{2} \times \frac{iter_k}{max_{iter}}\right) + \cos\left(\frac{\pi}{2} \times \frac{iter_k}{max_{iter}}\right) - 1\right) \tag{17}$$

Where δ denotes a random value ranged between [0,1], $iter_k$ denotes the current iteration, N denotes a fixed number which displays the procedure of the optimization and makes the investigation and process stages, max_{iter} denotes the overall number of iterations, and d indicates an amount that is limited between -2 and 2. If N falls below zero, the vulture is hungry, and if it rises over one, the vulture is fulfilled.

Stage3: Enquiry.

In this method vultures contain random segments with two potential designs and a variable R_1 with a value ranging from zero to one to determine the plane. The mathematical procedure for finding a meal for vultures is given in Eq. (18) and (19) as follows:

$If\ R_1 \geq randR_1$

$$S(k+1) = BV(k) - T(k) \times S \tag{18}$$

$If\ R_1 < randR_1$

$$S(k+1) = BV(k) - S + rand_2 \times ((ub - lb) \times rand_3 + lb \tag{19}$$

where S identifies the vultures that diverge from others at randomly in search of food., lb and ub are the variables' lower

and upper bounds, BV contains the best vultures, and $rand_2$ and $rand_3$ define two random standards among 0 and 1.

Stage 4: Utilization.

This happens if $|S| < 1$ divides the phase into two halves with two strategies that are determined by two R2 and R3 constraints that are in the range [0, 1]. The first portion of utilization begins at $0.5 < |S| < 1$. Both designs include rotational flights. If $|S| \geq 0.5$ indicates that a vulture is spirited; in this stage, weak bird attempt to ingest food on stronger vultures. $S(k+1)$ represents the vulture's present location and can be designed using Eq. (20), (21), (22) as follows:

$$S(k+1) = \frac{B_1 + B_2}{2} \quad (20)$$

Where,

$$B_1 = Best\ vulture_1(k) - \frac{Best\ vulture_1(k) \times S(k)}{Best\ vulture_1(k) - S(k)^2} \times S \quad (21)$$

$$B_2 = Best\ vulture_2(k) - \frac{Best\ vulture_2(k) \times S(k)}{Best\ vulture_2(k) - S(k)^2} \times S \quad (22)$$

The initial step of optimization is to specify the algorithm's minimal and maximum rate boundaries for avoiding system failures. The least acceptable value for the maximum pooling is taken to be 2, and the highest value is considered as moving width. The proposed CNN's half-value accuracy has been used as an objective function in this case. The algorithm was initialized, updated, and reached the end state before the procedure was ended. Weights and biases, which make up a CNN's main building blocks, are thought to be enhanced.

3) Skin cancer classification through Bi-LSTM: Bidirectional LSTM layers extract hidden and sequential features from images in both forward and reverse time directions. RNN involves memory and data storage limitations. It is incapable of learning long-term, which might lead to gradient disappearance. As a result, to overpower the insufficiencies of algorithm, the LSTM approach was devised. This construction is formed on the usage of memory cells which store long-term and gate mechanisms to control this information. A basic LSTM unit contains three types of gates: Input gate i_t, Forget gate m_t, and output gate o_t. Each gate controls the state of memory cells by executing point-wise multiplication and sigmoid operations on the image y_t. The architecture of LSTM is exposed in Fig. 4.

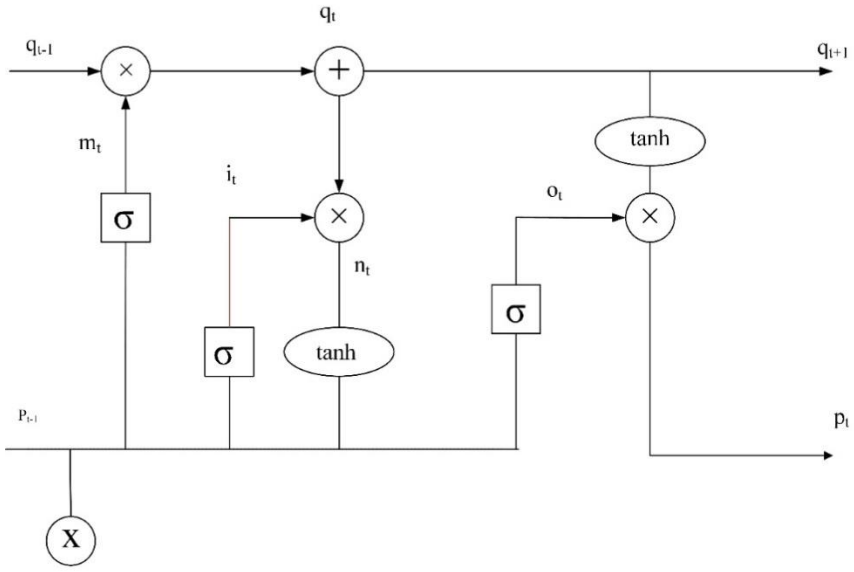

Fig. 4. LSTM architecture.

When input data y_t at its present state and output p_{t-1} from the preceding layer's hidden state are both entered, all gates are triggered. A forget gate specifies what information should be retained and which data should be ignored. The data gathered from the present input is used by sigmoid functions y_t to convey information from the present input $y_t$to the previous hidden state p_{t-1}. The forget gate's output value is between 0 and 1. When the rate is near to zero that indicates the data will be removed. More knowledge tends to be kept closer to oneself. The following procedures must be followed to calculate the forget gate formula using Eq. (23) input gate formula using Eq. (24) and output gate formula using Eq. (27) as follows:

$$m_t = \sigma(w_m . [p_{t-1}, y_t] + b_m) \quad (23)$$

$$i_t = \sigma(w_i . [p_{t-1}, y_t] + b_i \quad (24)$$

$$\hat{q}_t = \tanh(w_q . [p_{t-1}, y_t] + b_q) \quad (25)$$

Current state equation is expressed in eqn. (26),

$$q_t = m_t \odot q_{t-1} + i_t \odot \hat{q}_t \quad (26)$$

$$o_t = \sigma(w_o . [p_{t-1}, y_t] + b_o \quad (27)$$

Hidden state formula is given in eqn. (28),

$$p_t = o_t \odot \tanh(q_t) \quad (28)$$

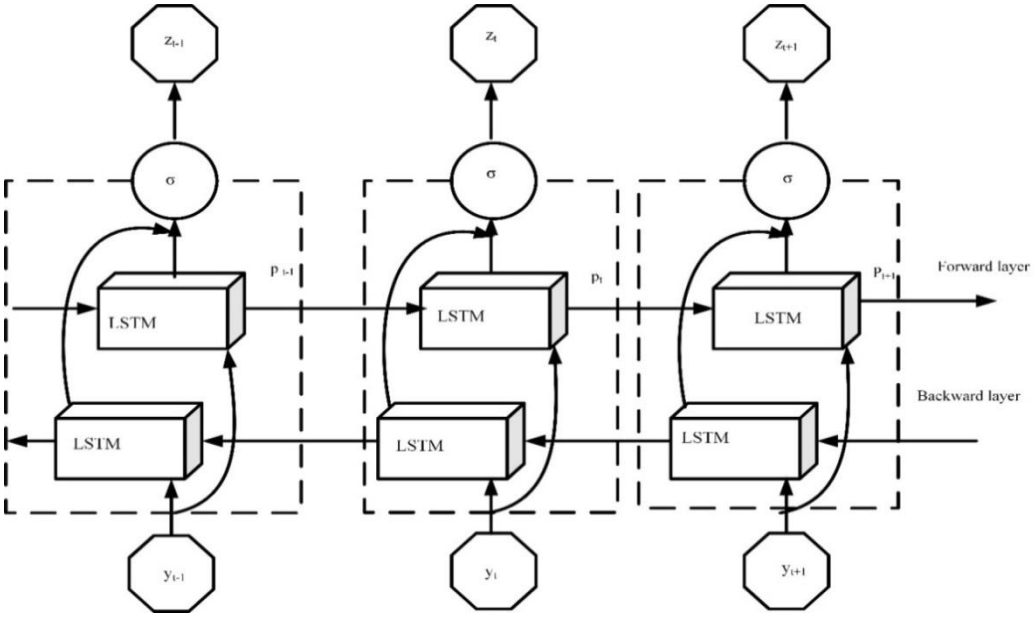

Fig. 5. Bi-LSTM architecture.

Bidirectional LSTM (Bi-LSTM) links the two LSTM hidden layers to the output layer. Combining two LSTM as a single layer stimulates enhance the learning long-term dependence and model performance. Fig. 5 depicts the structure of an unfolded Bi-LSTM layer with LSTM layer in forward and a backward direction. It classifies the input images as melanoma, benign and normal. Thus, the melanoma is detected from the input images.

GAN-AVO Algorithm

Input: Image containing skin lesion

Output: Melanoma detection in skin image

Load the input image

Image augmentation using GAN

Perform preprocessing operation *//contrast enhancement using CLAHE*

Noise removal using Weiner filter is given in eqn. (8)

Image segmentation *//compute threshold value using eqn. (10)*

Feature extraction *//color, border, diameter, shapes were extracted using CNN*

Select feature using AVO

Calculate the fitness of vultures

If(|s|≥1) then

Upgrade the location vulture using eqn. (19)

Else

Upgrade the location vulture using eqn. (20)

Endif

Classification using Bi-LSTM

End

The GAN-AVO algorithm is designed for the discovery of melanoma in skin lesion images. It begins by taking an input image containing a skin lesion and applies image augmentation through a Generative Adversarial Network (GAN) for data enhancement. Subsequently, the image undergoes preprocessing, involving contrast enhancement

using the CLAHE method and noise removal through a Weiner filter. Image segmentation is performed by computing a threshold value. To retrieve relevant features, a Convolutional Neural Network (CNN) is employed to capture color, border, diameter, and shape information. AVO is utilized to select pertinent features, followed by the computation of fitness for vultures. If the number of selected features (|s|) is greater than or equal to 1, the algorithm upgrades vulture locations using Eq. (19); otherwise, it utilizes Eq. (20). Finally, the algorithm employs a Bi-LSTM network for classification, culminating in melanoma detection. This comprehensive approach integrates GAN-based augmentation, preprocessing, segmentation, feature extraction, AVO feature selection, and Bi-LSTM classification to effectively identify melanoma in skin lesion images. Fig. 6 shows flowchart of this research.

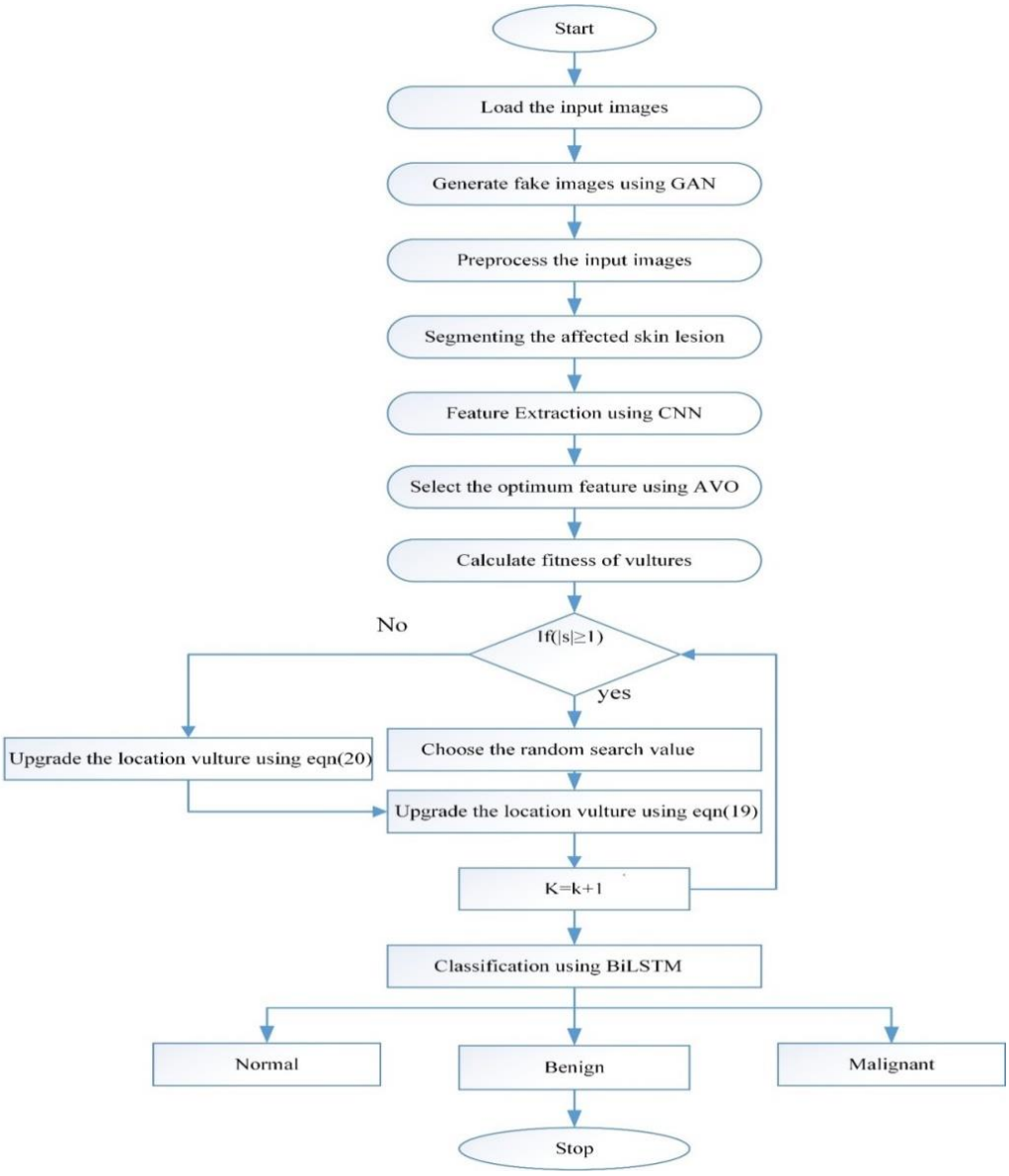

Fig. 6. Flowchart of proposed method.

V. RESULTS

The proposed study aimed to enhance the accuracy of melanoma detection in skin images by employing a novel AI driven African Vulture optimization with GAN based Bi-LSTM deep framework for melanoma detection. The approach used GANs to create realistic and variety fake images, which were then mixed with the original dataset to supplement training images and improve model generalisation. AVO was used to optimise the network design and hyperparameters, improving the model's overall performance. Extensive tests on a large-scale image were carried out, and the findings showed a considerable improvement in skin cancer diagnosis and localization accuracy. The following metric was used to assess the model efficiency of the strategy.

For comparison, the following segmentation of skin lesion evaluation criteria was used: precision, recall, F1-score, and accuracy. These parameters were used to assess the model. These are depicted below:

Accuracy: It calculates the fraction of real outcomes including true positives and true negatives across all cases investigated. It is expressed in Eq. (29),

$$Accuracy = \frac{TP+TN}{TP+TN+FP+FN} \quad (29)$$

Precision: The ratio of exactly anticipated positive outcomes to overall predicted positive occurrences is defined as precision. The precision is calculated using Eq. (30).

$$Precision = \frac{TP}{TP+FP} \quad (30)$$

Recall: The recall measures the proportion of genuine positive samples that were projected to be positive. Using Eq. (31), calculate the value recall.

$$Recall = \frac{TP}{TP+FN} \quad (31)$$

where, FP represents false positive pixels, FN signifies false negative pixels, TP symbolizes true positive pixels, and TN describes true negative pixels.

F1-score: In the categorization task, recall and accuracy relate to one another. Although a high value for both is ideal, the reality is generally great accuracy with low recall, or high recall with low accuracy. To account for both recollection and accuracy, the F1-score, which is a mean of recall and accuracy, can be employed. Eq. (32) shows the definition of F1-score.

$$F1-score = 2 * \frac{Precision*Recall}{Precision+Recall} \quad (32)$$

TABLE I. PERFORMANCE METRICS OF PROPOSED METHOD

Proposed GAN-BiLSTM with AVO	
Performance Metrics	**Values (%)**
Accuracy	98.5
Precision	98.1
Recall	98
F1-score	98

The assessment results of the created skin cancer detection system employing the combined strategy are shown in Table I. At 98.5%, the accuracy is exceptionally high. Precision, which measures the percentage of accurate positive predictions compared to all positive forecasts, is an outstanding 98.1%. The system's capacity to accurately detect real positive cases is demonstrated by the recall measure, also known as sensitivity which is remarkably high at 98%. At 98%, the F1-score, which balances recall and accuracy, is very impressive.

With high values across key performance parameters, these findings show precise and reliable skin cancer diagnosis. Fig. 7 illustrates the performance assessment of proposed GAN-Bi-LSTM with AVO.

Table II shows the Accuracy, Recall Precision and F1-score of the proposed approach with existing methods. The accuracy of the suggested method GAN-Bi-LSTM with AVO (98.5%) is higher than the existing approaches convnet (91.03%), Inception RESNET (91%) and RESNET-18(94.47%). Fig. 8 depicts the graphic depiction of the performance metrics of proposed with existing approaches. The precision of the suggested method GAN-Bi-LSTM with AVO (98.1%) is higher than the existing approaches convnet (91.09%), Inception RESNET (91%) and RESNET-18(93.57%). The recall of the suggested method GAN-Bi-LSTM with AVO (98%) is higher than the existing approaches convnet (90.96%), Inception RESNET (91%) and RESNET-18(94.01%). The F1-score of the suggested method GAN-Bi-LSTM with AVO (98%) is higher than the existing approaches convnet (91.01%), Inception RESNET (91%) and RESNET-18(94.45%).

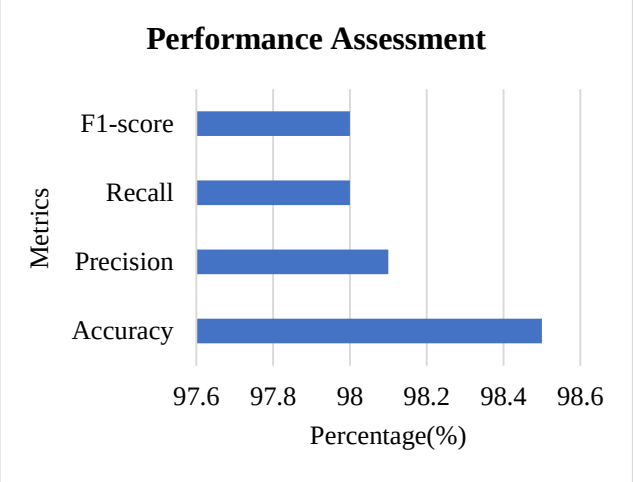

Fig. 7. Performance assessment of proposed GAN-Bi-LSTM with AVO.

TABLE II. PERFORMANCE METRICS OF PROPOSED METHOD IS EVALUATED WITH EXISTING METHODS

Methods	**Accuracy (%)**	**Precision (%)**	**Recall (%)**	**F1-score (%)**
Convnet [28]	91.03	91.09	90.96	91.01
Inception RESNET [29]	91	91	91	91
RESNET-18 [30]	94.47	93.57	94.01	94.45
Proposed method	98.5	98.1	98	98

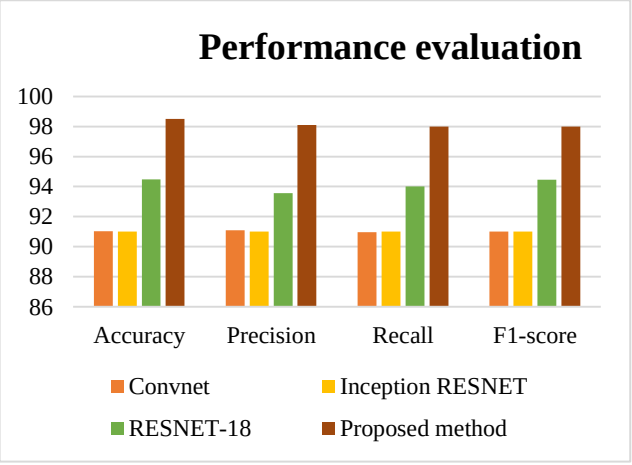

Fig. 8. Graphical illustration of the performance metrics of proposed with existing approaches.

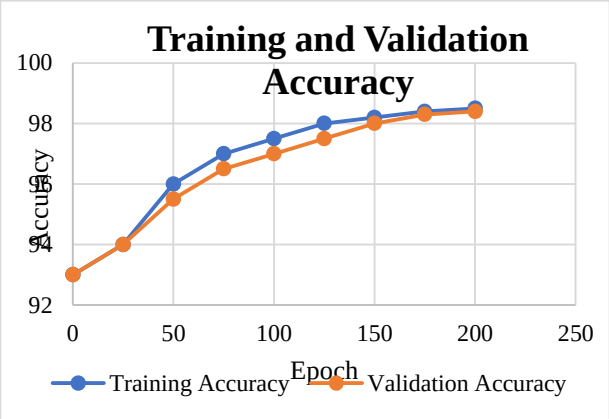

Fig. 9. Graphical depiction for training and validation accuracy of proposed method.

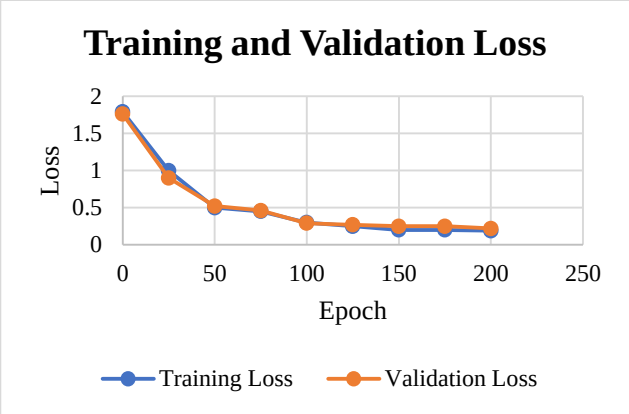

Fig. 10. Graphical representation of loss in proposed AVO-Bi-LSTM.

The accuracy level and loss rates fluctuation graphs for the entire GAN-based AVO-Bi-LSTM model procedure are displayed in Fig. 9 and 10. The accuracy ratio and loss ratio overall graph has stabilized at the training intervals of the GAN-based AVO-Bi-LSTM are at 100, and it is clear that the GAN-based AVO-Bi-LSTM fits data more quickly.

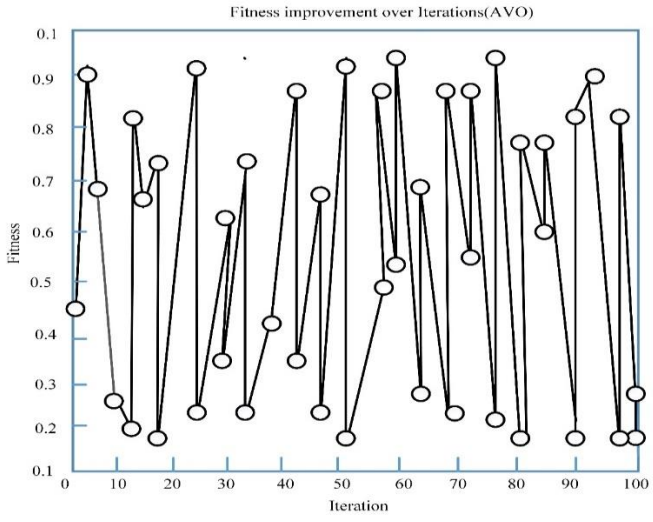

Fig. 11. Fitness improvement over iterations (AVO).

Before optimisation the value of accuracy for proposed GAN based AVO-Bi-LSTM is 98%. The accuracy achieved after optimisation using AVO is 98.5%. The fitness of AVO is depicted in Fig. 11. Using Eq. (33), the Area Under the Curve (AUC) has been calculated to estimate AVO-Bi-LSTM's overall performance. Fig. 12 shows ROC curve for the GAN-based AVO-Bi-LSTM model, and it can be seen that the ROC area is nearly close to 1, confirming the model's good stability and potential for usage as classification model for skin cancer diagnosis.

$$AUC = \frac{1}{2}\left(\frac{TP}{TP+FN} + \frac{TN}{TN+FP}\right) \quad (33)$$

AUC of proposed GAN based AVO-Bi-LSTM is compared with existing model (mAlexNet + Bi-LSTM) is given in Table III.

TABLE III. AUC OF PROPOSED GAN BASED AVO-BI-LSTM IS COMPARED WITH EXISTING MODEL

Architecture	AUC
mAlexNet + Bi-LSTM	0.97
Proposed AVO + Bi-LSTM	0.985

In Table III, two distinct architectures are evaluated for their melanoma detection capabilities. The first architecture, which combines modified AlexNet (mAlexNet) with a Bi-LSTM network, achieves an Area Under the Curve (AUC) of 0.97. This indicates a strong ability of the mAlexNet and Bi-LSTM combination to victimize melanoma. In comparison, the proposed approach, utilizing Artificial Vulture Optimization (AVO) for feature selection in conjunction with a Bi-LSTM network, outperforms the former with an AUC of 0.985. The higher AUC value achieved by the proposed AVO + Bi-LSTM architecture underscores its superior ability to effectively distinguish melanoma cases from non-melanoma instances, highlighting its potential as an advanced and promising model for accurate melanoma detection in skin lesion images.

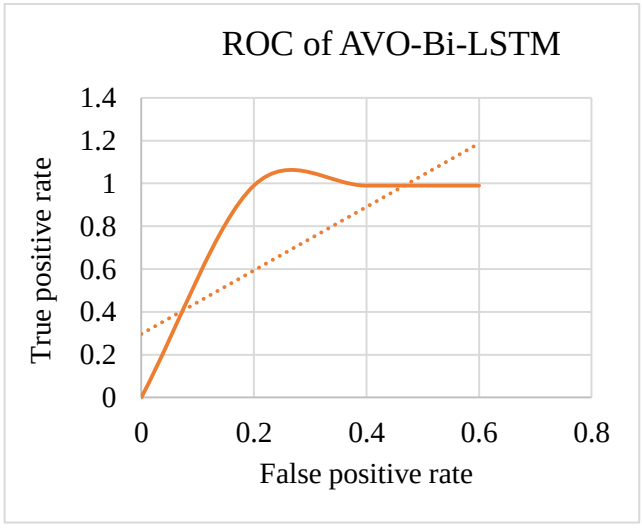

Fig. 12. ROC curve for proposed AVO-Bi-LSTM.

A. Discussion

The proposed study aimed to significantly enhance the accuracy of melanoma detection in skin images by employing a novel AI-driven approach combining African Vulture optimization (AVO) with a Generative Adversarial Network (GAN)-based Bidirectional Long Short-Term Memory (Bi-LSTM) deep framework. This innovative approach harnessed GANs to generate realistic and diverse synthetic images, augmenting the original dataset to improve model generalization. AVO was utilized to optimize network design and hyperparameters, resulting in a substantial boost in the overall performance of the model. Extensive testing on a large-scale image dataset yielded highly promising results, showcasing a remarkable improvement in skin cancer diagnosis and localization accuracy. The evaluation of the model's efficiency was based on standard segmentation criteria, including precision, recall, F1-score, and accuracy. The results were exceptionally favorable, with an accuracy rate of 98.5%, precision at 98.1%, recall reaching 98%, and an impressive F1-score of 98%, indicating the model's precision and reliability in skin cancer diagnosis.

Comparing the proposed approach with existing methods, the superiority of the GAN-Bi-LSTM with AVO method was evident. Its accuracy of 98.5% outperformed other methods such as Convnet (91.03%), Inception RESNET (91%), and RESNET-18 (94.47%). Similarly, the precision, recall, and F1-score of the proposed method were significantly higher than those of existing methods, reaffirming its effectiveness in accurate melanoma detection. Visual representations of performance metrics, as depicted in Fig. 7, 8, 9, and 10, further illustrated the consistent and stable performance of the GAN-Bi-LSTM with AVO model. Moreover, AVO optimization yielded an even higher accuracy of 98.5%, compared to the initial accuracy of 98%, as shown in Fig. 11. The Area Under the Curve (AUC) analysis also indicated the superiority of the proposed AVO + Bi-LSTM architecture over an existing model, with an AUC of 0.985 compared to 0.97, underscoring its potential as an advanced and reliable model for accurate melanoma detection in skin lesion images.

VI. Conclusion

The research introduces an AI-powered framework that combines African Vulture Optimization with Generative Adversarial Networks (GANs) and Bidirectional Long Short-Term Memory (Bi-LSTM) networks for melanoma detection. This study serves as an illustrative example of Bi-LSTM's application in identifying skin cancer from lesion images. GANs are harnessed to address data imbalance, generating additional data to enhance detection. Furthermore, the research devises an ensemble model that synergizes Bi-LSTM and GANs, surpassing the performance of the standalone deep learning model. Employing an iterative AVO evolutionary method enhances a population of solutions via fitness assessment. Depending on outcomes, this approach could potentially outperform existing artificial intelligence methods. Ultimately, the proposed hybrid deep learning framework, incorporating GANs and AV optimization, notably improves the accuracy of skin cancer detection and localization within skin images. The integration of GANs and AV optimization effectively tackles data limitations and optimizes deep learning models, contributing to the advancement of melanoma diagnosis. The future work explores the integration of other imaging modalities, such as dermoscopy or infrared imaging, alongside the proposed framework to enhance the model's ability to detect melanoma across various imaging sources.

References

[1] R. Ashraf et al., “Region-of-Interest Based Transfer Learning Assisted Framework for Skin Cancer Detection,” IEEE Access, vol. 8, pp. 147858–147871, 2020, doi: 10.1109/ACCESS.2020.3014701.

[2] M. S. Khan, K. N. Alam, A. R. Dhruba, H. Zunair, and N. Mohammed, “Knowledge Distillation approach towards Melanoma Detection,” Comput. Biol. Med., vol. 146, p. 105581, Jul. 2022, doi: 10.1016/j.compbiomed.2022.105581.

[3] D. Adla, G. V. R. Reddy, P. Nayak, and G. Karuna, “Deep learning-based computer aided diagnosis model for skin cancer detection and classification,” Distrib. Parallel Databases, vol. 40, no. 4, pp. 717–736, Dec. 2022, doi: 10.1007/s10619-021-07360-z.

[4] A. Adegun and S. Viriri, “Deep learning techniques for skin lesion analysis and melanoma cancer detection: a survey of state-of-the-art,” Artif. Intell. Rev., vol. 54, no. 2, pp. 811–841, Feb. 2021, doi: 10.1007/s10462-020-09865-y.

[5] M. Deb Barma, M. A. Indiran, P. Kumar R, A. Balasubramaniam, and M. P. S. Kumar, “Quality of life among head and neck cancer treated patients in South India: A cross-sectional study,” J. Oral Biol. Craniofacial Res., vol. 11, no. 2, pp. 215–218, Apr. 2021, doi: 10.1016/j.jobcr.2021.02.002.

[6] K. Thurnhofer-Hemsi and E. Domínguez, “A Convolutional Neural Network Framework for Accurate Skin Cancer Detection,” Neural Process. Lett., vol. 53, no. 5, pp. 3073–3093, Oct. 2021, doi: 10.1007/s11063-020-10364-y.

[7] S. Banerjee, S. K. Singh, A. Chakraborty, A. Das, and R. Bag, “Melanoma Diagnosis Using Deep Learning and Fuzzy Logic,” Diagnostics, vol. 10, no. 8, p. 577, Aug. 2020, doi: 10.3390/diagnostics10080577.

[8] A. Naeem, M. S. Farooq, A. Khelifi, and A. Abid, “Malignant Melanoma Classification Using Deep Learning: Datasets, Performance Measurements, Challenges and Opportunities,” IEEE Access, vol. 8, pp. 110575–110597, 2020, doi: 10.1109/ACCESS.2020.3001507.

[9] R. M Abd El-Aziz et al., “An Effective Data Science Technique for IoT-Assisted Healthcare Monitoring System with a Rapid Adoption of Cloud Computing,” Comput. Intell. Neurosci., vol. 2022, pp. 1–9, Jan. 2022, doi: 10.1155/2022/7425846.

[10] L. Ichim and D. Popescu, “Melanoma Detection Using an Objective System Based on Multiple Connected Neural Networks,” IEEE Access, vol. 8, pp. 179189–179202, 2020, doi: 10.1109/ACCESS.2020.3028248.

[11] J. K. Winkler et al., “Melanoma recognition by a deep learning convolutional neural network—Performance in different melanoma subtypes and localisations,” Eur. J. Cancer, vol. 127, pp. 21–29, Mar. 2020, doi: 10.1016/j.ejca.2019.11.020.

[12] M. Nawaz et al., “Skin cancer detection from dermoscopic images using deep learning and fuzzy k -means clustering,” Microsc. Res. Tech., vol. 85, no. 1, pp. 339–351, Jan. 2022, doi: 10.1002/jemt.23908.

[13] M. Toğaçar, Z. Cömert, and B. Ergen, “Intelligent skin cancer detection applying autoencoder, MobileNetV2 and spiking neural networks,” Chaos Solitons Fractals, vol. 144, p. 110714, Mar. 2021, doi: 10.1016/j.chaos.2021.110714.

[14] H. U. Rehman, N. Nida, S. A. Shah, W. Ahmad, M. I. Faizi, and S. M. Anwar, “Automatic melanoma detection and segmentation in dermoscopy images using deep RetinaNet and conditional random fields,” Multimed. Tools Appl., vol. 81, no. 18, pp. 25765–25785, Jul. 2022, doi: 10.1007/s11042-022-12460-8.

[15] B. A. Albert, “Deep Learning From Limited Training Data: Novel Segmentation and Ensemble Algorithms Applied to Automatic Melanoma Diagnosis,” IEEE Access, vol. 8, pp. 31254–31269, 2020, doi: 10.1109/ACCESS.2020.2973188.

[16] S. Jiang, H. Li, and Z. Jin, "A Visually Interpretable Deep Learning Framework for Histopathological Image-Based Skin Cancer Diagnosis," IEEE J. Biomed. Health Inform., vol. 25, no. 5, pp. 1483–1494, May 2021, doi: 10.1109/JBHI.2021.3052044.

[17] M. Shorfuzzaman, "An explainable stacked ensemble of deep learning models for improved melanoma skin cancer detection," Multimed. Syst., vol. 28, no. 4, pp. 1309–1323, Aug. 2022, doi: 10.1007/s00530-021-00787-5.

[18] L. Wei, K. Ding, and H. Hu, "Automatic Skin Cancer Detection in Dermoscopy Images Based on Ensemble Lightweight Deep Learning Network," IEEE Access, vol. 8, pp. 99633–99647, 2020, doi: 10.1109/ACCESS.2020.2997710.

[19] X. Wang, X. Jiang, H. Ding, Y. Zhao, and J. Liu, "Knowledge-aware deep framework for collaborative skin lesion segmentation and melanoma recognition," Pattern Recognit., vol. 120, p. 108075, Dec. 2021, doi: 10.1016/j.patcog.2021.108075.

[20] A. A. Adegun and S. Viriri, "Deep Learning-Based System for Automatic Melanoma Detection," IEEE Access, vol. 8, pp. 7160–7172, 2020, doi: 10.1109/ACCESS.2019.2962812.

[21] M. Manzo and S. Pellino, "Bucket of Deep Transfer Learning Features and Classification Models for Melanoma Detection," J. Imaging, vol. 6, no. 12, p. 129, Nov. 2020, doi: 10.3390/jimaging6120129.

[22] S. İlkin, T. H. Gençtürk, F. Kaya Gülağız, H. Özcan, M. A. Altuncu, and S. Şahin, "hybSVM: Bacterial colony optimization algorithm based SVM for malignant melanoma detection," Eng. Sci. Technol. Int. J., vol. 24, no. 5, pp. 1059–1071, Oct. 2021, doi: 10.1016/j.jestch.2021.02.002.

[23] R. V. Selvarani and P. S. H. Jose, "A Label-Free Marker Based Breast Cancer Detection using Hybrid Deep Learning Models and Raman Spectroscopy," Trends Sci., vol. 20, no. 4, p. 6299, Jan. 2023, doi: 10.48048/tis.2023.6299.

[24] W. Gouda, N. U. Sama, G. Al-Waakid, M. Humayun, and N. Z. Jhanjhi, "Detection of Skin Cancer Based on Skin Lesion Images Using Deep Learning," Healthcare, vol. 10, no. 7, p. 1183, Jun. 2022, doi: 10.3390/healthcare10071183.

[25] R. Fan, X. Li, S. Lee, T. Li, and H. L. Zhang, "Smart Image Enhancement Using CLAHE Based on an F-Shift Transformation during Decompression," Electronics, vol. 9, no. 9, p. 1374, Aug. 2020, doi: 10.3390/electronics9091374.

[26] M. Dhanushree, R. Priyadharsini, and T. Sree Sharmila, "Acoustic image denoising using various spatial filtering techniques," Int. J. Inf. Technol., vol. 11, no. 4, pp. 659–665, Dec. 2019, doi: 10.1007/s41870-018-0272-3.

[27] L. Hu, Y. Zhang, K. Chen, and S. Mobayen, "A COMPUTER-AIDED melanoma detection using deep learning and an improved African vulture optimization algorithm," Int. J. Imaging Syst. Technol., vol. 32, no. 6, pp. 2002–2016, Nov. 2022, doi: 10.1002/ima.22738.

[28] Q. Abbas, F. Ramzan, and M. U. Ghani, "Acral melanoma detection using dermoscopic images and convolutional neural networks," Vis. Comput. Ind. Biomed. Art, vol. 4, no. 1, p. 25, Dec. 2021, doi: 10.1186/s42492-021-00091-z.

[29] H. Nahata and S. P. Singh, "Deep Learning Solutions for Skin Cancer Detection and Diagnosis," in Machine Learning with Health Care Perspective, V. Jain and J. M. Chatterjee, Eds., in Learning and Analytics in Intelligent Systems, vol. 13. Cham: Springer International Publishing, 2020, pp. 159–182. doi: 10.1007/978-3-030-40850-3_8.

[30] N. Nigar, M. Umar, M. K. Shahzad, S. Islam, and D. Abalo, "A Deep Learning Approach Based on Explainable Artificial Intelligence for Skin Lesion Classification," IEEE Access, vol. 10, pp. 113715–113725, 2022, doi: 10.1109/ACCESS.2022.3217217.